Design and Numerical Evaluation of Cascade-Type Thermoelectric Modules

Takeyuki Fujisaka, Hongtao Sui, and Ryosuke O. Suzuki

Faculty of Engineering, Hokkaido University, Sapporo, Hokkaido 060-8628, Japan

TEL: +81-11-706-6341

FAX: +81-11-706-6342

fujisaka@eng.hokudai.ac.jp

Abstract

Thermoelectric (TE) generation performance can be enhanced by stacking several TE modules (so-called cascade-type modules). This work presents a design method to optimize the cascade structure for maximum power output. A one-dimensional model was first analyzed to optimize the TE element dimensions by considering the heat balance including conductive heat transfer, Peltier heat, and Joule heat, assuming constant temperatures at all TE junctions. The number of p-n pairs was successively optimized to obtain maximum power. The power output increased by 1.24 times; from 12.7 W in a conventional model to 15.7 W in an optimized model. Secondly, a two-dimensional numerical calculation based on the finite volume method was used to evaluate the temperature and electric potential

distributions. Voltage-current characteristics were calculated, the maximum power output was evaluated, and the efficiencies of two possible models were compared to select the optimal design. The one-dimensional analytical approach is effective for a rough design, and the multi-dimensional numerical calculation is effective for evaluating the dimensions and performance of a cascade-type TE module in detail.

Keywords

Thermoelectric generation, cascade module, numerical simulation, optimization, heat transfer

NOMENCLATURE

T	Temperature (K)
Q_h	Heat transfer rate from heat source to hot surface of cascade module (W)
Q_c	Heat transfer rate from cold surface of cascade module to heat sink (W)
P	Output power of cascade module (W)
η	Conversion efficiency (-); = P/Q_h

n	Number of p-n pairs in single stage module (-)
m	Number of stages in multi-stage cascade module (-)
d	Leg length of TE element (m)
a	Cross-sectional area of TE element (m^2)
l	Ratio of a to d (m); = a/d
S	Relative Seebeck coefficient ($V K^{-1}$)
ρ	Electric resistivity (Ω m)
λ	Thermal conductivity ($W m^{-1} K^{-1}$)
K	Thermal conductance ($W K^{-1}$)
R	Electric resistance (Ω)
R_L	External load (Ω)
I	Current (A)
E	Electromotive force (V)
V	Electric potential (V)
$\boldsymbol{J}$	Current density ($A m^{-2}$)

Subscript

i	*i* th stage from hot side in multi-stage cascade module

Superscripts

p	*p*-type material
n	*n*-type material

1 INTRODUCTION

Thermoelectric (TE) generation based on the Seebeck effect can directly convert heat into electricity. A TE generation system has the advantage of not requiring a large-scale system and has been studied as a way to recover unused heat, such as waste heat from automobiles [1], fuel cells [2], and marine engines [3], as well as solar heat [4,5]. However, the conversion efficiency of TE generation systems is generally low.

TE generation efficiency is determined by the working temperature and material properties, and the TE power is generally proportional to the square of the temperature difference. However, conventional single-stage TE modules operating under large temperature difference conditions cannot effectively convert heat to power because

there are no TE materials that maintain a good performance over a wide temperature range.

The performance can be enhanced by stacking several TE modules (so-called cascade modules) [6-8]. The cascade TE generation efficiency can be increased by using materials suitable for the working temperature range. Another method to improve the efficiency is to optimize the module structure parameters, such as the TE element size and number of p-n pairs.

Harman [6] derived a general expression for the overall efficiency of multi-stage cascade modules and the optimal p-n pair number ratio in a two-stage module for a given intermediate junction temperature by using a one-dimensional (1D) heat balance model. In a practical module construction, Zhang et al. [7] indicated that cascade TE generators using TE oxides have a high potential for heat recovery from high-temperature waste. Funahashi [8] fabricated cascade modules consisting of oxide and Bi_2Te_3 modules and indicated experimentally that cascade structures are effective for high efficiency. Kaibe et al. [9] showed that the efficiency is as high as 10% using TE silicide and Bi_2Te_3. Although cascade design has been the subject of some research for an extended time, the optimal structure remains elusive and understudied.

The purpose of this work is to optimize the cascade module structure and highlight the key design points. Calculation results of cascade structures using 1D analytical and two-dimensional (2D) numerical calculations of the temperature distribution are presented. The TE element dimensions and number of p-n pairs were firstly optimized through the 1D analysis to obtain the maximum power output, and this was followed by numerical calculations based on the finite volume method to optimize the TE element sizes and evaluate the efficiencies of the two possible models proposed in the 1D analysis.

2 MODELING

2.1 ONE-DIMENSIONAL ANALYTICAL MODEL AND EVALUATION PROCEDURE

Figure 1 illustrates a cascade module consisting of *m* stages. It is assumed that the input heat on the top surface, Q_h, is transferred to a heat sink without any energy loss, such as that caused by thermal or electric contact resistance, and that the thermal resistance of the electric insulators can be ignored. The heat balance equations [6, 10] are written as

$$
\begin{cases}
Q_{\mathrm{h}} = \left[K_1 (T_0 - T_1) + S_1 T_0 I - \dfrac{1}{2} R_1 I^2 \right] n_1 \\
\quad \vdots \\
\left[K_{m-1} (T_{m-2} - T_{m-1}) + S_{m-1} T_{m-1} I + \dfrac{1}{2} R_{m-1} I^2 \right] n_{m-1} \\
\quad = \left[K_m (T_{m-1} - T_m) + S_m T_{m-1} I - \dfrac{1}{2} R_m I^2 \right] n_m \\
Q_{\mathrm{c}} = \left[K_m (T_{m-1} - T_m) + S_m T_m I + \dfrac{1}{2} R_m I^2 \right] n_m
\end{cases} \tag{1}
$$

where $K_i(T_{i-1}-T_i)$, S_iT_iI, and $(1/2)R_iI^2$ represent the heat conduction, Peltier heat, and Joule heat, respectively, of one p-n pair. The terms K_i and R_i are

$$K_i = \lambda_i^{\mathrm{p}} \frac{a_i^{\mathrm{p}}}{d_i} + \lambda_i^{\mathrm{n}} \frac{a_i^{\mathrm{n}}}{d_i} = \lambda_i^{\mathrm{p}} l_i^{\mathrm{p}} + \lambda_i^{\mathrm{n}} l_i^{\mathrm{n}} \tag{2}$$

$$R_i = \rho_i^{\mathrm{p}} \frac{d_i}{a_i^{\mathrm{p}}} + \rho_i^{\mathrm{n}} \frac{d_i}{a_i^{\mathrm{n}}} = \frac{\rho_i^{\mathrm{p}}}{l_i^{\mathrm{p}}} + \frac{\rho_i^{\mathrm{n}}}{l_i^{\mathrm{n}}} \tag{3}$$

In order to maximize the conversion efficiency under constant temperature conditions, the optimal relationship between l_i^{p} and l_i^{n} [6, 10] is given by

$$\frac{l_i^{\mathrm{n}}}{l_i^{\mathrm{p}}} = \sqrt{\frac{\rho_i^{\mathrm{n}} \lambda_i^{\mathrm{p}}}{\rho_i^{\mathrm{p}} \lambda_i^{\mathrm{n}}}} \tag{4}$$

Thus, using Eq. (4), Eq. (2) and (3) can be rewritten as

$$K_i = \left(\lambda_i^{\mathrm{p}} + \lambda_i^{\mathrm{n}} \sqrt{\frac{\rho_i^{\mathrm{n}} \lambda_i^{\mathrm{p}}}{\rho_i^{\mathrm{p}} \lambda_i^{\mathrm{n}}}} \right) l_i^{\mathrm{p}} \tag{5}$$

$$R_i = \left(\rho_i^{\mathrm{p}} + \rho_i^{\mathrm{n}} \sqrt{\frac{\rho_i^{\mathrm{p}} \lambda_i^{\mathrm{n}}}{\rho_i^{\mathrm{n}} \lambda_i^{\mathrm{p}}}} \right) \frac{1}{l_i^{\mathrm{p}}} \tag{6}$$

It is noteworthy that the variable parameter related to the TE element dimensions is only l_i^{p}, and l_i^{n} is automatically determined by Eq. (4).

A practical assumption is taken here that all modules are connected electrically in series because a series circuit has the advantage that the number of output electric leads is reduced to only two and that the heat loss from the leads can be minimized compared with parallel and individual connections. The current and electromotive force are then given by

$$I = \frac{\sum_{i=1}^{m} n_i S_i \left(T_{i-1} - T_i\right)}{R_{\mathrm{L}} + \sum_{i=1}^{m} n_i R_i} \qquad (7)$$

$$E = \sum_{i=1}^{m} n_i S_i \left(T_{i-1} - T_i\right) - \sum_{i=1}^{m} n_i R_i I \qquad (8)$$

It is assumed that Q_{h}, Q_{c}, T_0, ..., T_m, l_1^{p}, ..., l_m^{p}, and n_1, ..., n_m are variables in the m-stage cascade model. The number of free variables then totals $3m + 3$, while the number of parameters is fixed at $m + 1$ in Eq. (1). Therefore, $2m + 2$ of these $3m + 3$ variables can be freely set as target values. Although the junction temperatures T_0, ..., T_m are generally unknown, they were fixed as target temperature assumptions in this work. In addition, n_1, ..., n_m and Q_{h} were fixed as external variables. Under these conditions, l_1^{p}, ..., l_m^{p} and Q_{c} were solved by applying Eq. (1). When each stage of a cascade module is connected electrically in series, the optimization of number of p-n pairs is needed to optimize the

relation between electromotive force and internal resistance of a module in order to enhance the conversion efficiency. Of course the optimal dimensions of TE elements depend on the number of p-n pairs, and these two parameters need to be optimized simultaneously.

The output power of the module is defined as

$$P = Q_{\mathrm{h}} - Q_{\mathrm{c}} = IE \qquad (9)$$

and the maximum power $P_{\max}$ [10] is given by

$$P_{\max} = \frac{\left(\sum_{i=1}^{m} n_i S_i \left(T_{i-1} - T_i \right) \right)^2}{4 \sum_{i=1}^{m} n_i R_i} \qquad (10)$$

where the external resistance is optimized. The power was calculated by repeatedly varying n_1, ..., n_m in order to find optimal values. In practice, the variation in the number of pairs brings out some complicated issues such as arrangement of TE elements and size of empty space between the elements, which affect heat transfer rate Q_{h} or Q_{c}. However, those issues that should be considered in two- or three-dimensional model are neglected because one-dimensional heat transfer model is considered in this section.

2.2 NUMERICAL MODEL AND EVALUATION PROCEDURE

In the 1D model, only the heat balance at the junctions is considered, and we have no knowledge about the temperature or current density distribution inside the TE materials because a differential equation for the heat conduction is not included. Taking energy conservation inside a control volume into consideration, the heat conduction equation under steady-state conditions [11] is written as

$$\nabla \cdot \left(\lambda \nabla T\right) + \rho \left|\boldsymbol{J}\right|^2 - T\boldsymbol{J} \cdot \nabla S = 0 \qquad (11)$$

where the first, second, and third terms represent the heat conduction, Joule heat generated by the current along the control volume, and heating or cooling generated by the Thomson effect, respectively. The current density $\boldsymbol{J}$ is related to the electric potential and temperature as [11]

$$\rho \boldsymbol{J} = -\nabla V - S\nabla T \qquad (12)$$

where the first term on the right-hand side is the voltage drop due to Ohm's law, and the second term is the increase in voltage generated by the Seebeck effect. The following differential equation can be derived from Eq. (12) by applying charge conservation under steady-state conditions ($\nabla \cdot \boldsymbol{J}=0$).

$$\nabla \cdot \left(-\frac{1}{\rho} \nabla V \right) = \nabla \cdot \left(\frac{S}{\rho} \nabla T \right) \qquad (13)$$

The temperature and electric potential distributions can be obtained by solving the simultaneous differential equations of Eq. (11) and (13). However, it is extremely difficult to find an analytical solution, except for the simplest conditions. In this work, the equations were solved numerically based on the finite volume method by modifying the commercial software ANSYS FLUENT. The detailed algorithm and method for applying the TE numerical model to FLUENT were reported in Ref. [11, 12], and the TE model was demonstrated in previous studies [3, 13]. However, the numerical model here is not completely consistent with Ref. [11]. The transport equations were solved for user-defined scalars (UDSs) in FLUENT, which can then be used to solve Eq. (12). One UDS is used to represent Eq. (13) in this work, while two UDSs were used in Ref. [11] to represent the two terms on the right-hand side of Eq. (12).

Figure 2 shows the workflow of the numerical calculation. After giving the initial values such as the temperature and electric potential distributions and the boundary conditions, the terms induced by thermoelectric phenomena were evaluated. Subsequently, Eq. (11) and (13) were solved, and temperature and electric potential

distributions were obtained. By updating the source terms and boundary conditions with the results, FLUENT iterates the procedure until the solution converges.

3 RESULTS AND DISCUSSION

3.1 ONE-DIMENSIONAL ANALYTICAL EVALUATION

In this section, we focus on three-stage (m = 3) cascade modules. Table 1 shows the TE material combinations that our team intends to apply to practical TE modules [8, 10, 14-17]. Cases 1 and 2 are recently obtained experimental data, and Case 3 is the ideal target data. In the 1D analytical calculations, the temperature dependencies of the TE properties are ignored. Using these three examples, we attempted to optimize the TE material dimensions and number of p-n pairs. The thermal conditions were set to Q_h = 400 kW/m^2, T_0 = 1200 K, T_1 = 800 K, T_2 = 500 K, and T_3 = 300 K. In addition, n_2 and n_3 were varied and n_1 = 100 for all calculations.

Figures 3 (a), (b), and (c) show contour plots of the efficiency against n_2 and n_3 for Cases 1, 2, and 3, respectively. There is a clear optimal set of n_2 and n_3 for the corresponding n_1 value. Cases 1-A, 2-A, and 3-A indicate the traditional cascade

module design ($n_1 = n_2 = n_3$), and Cases 1-B, 2-B, and 3-B are the optimized conditions found in this work. Table 2 summarizes the results for the optimized conditions.

Comparing Cases 1-B, 2-B, and 3-B, it is clear that the optimal condition depends on the TE material combination. When materials with a higher performance are used, the optimization procedure becomes crucial and is effective in enhancing the conversion efficiency. Additionally, the optimization of the TE element dimensions (l_1^{p}, l_2^{p}, and l_3^{p}) is needed to obtain the target temperature distribution. Therefore, in designing a cascade module, it is not satisfactory to simply select high-performance TE materials; the structure should also be designed with the optimal length, cross-sectional area, and number of p-n pairs.

3.2 TWO-DIMENSIONAL NUMERICAL EVALUATION

In the 1D analytical procedure, both the number of p-n pairs and the TE element dimensions were optimized. However, the dimension optimization is not ideal because, although l is optimized, both a and d are not individually determined. In order to optimize these parameters, a two- or three-dimensional analysis is effective.

In this section, we focus on two-stage (m = 2) cascade modules to simplify the problem. A temperature range of 300–800 K is assumed for comparison with the 1D results, and Case 1 is used. In the numerical analysis, we also include electrodes and insulators made of copper (0.2 mm thick) and alumina (0.6 mm thick), respectively. Their properties are taken from Ref. [18]. Both thermal and electric contact resistances are ignored. The arrangement of p-n elements and the size of empty space between the elements were determined and fixed by reference to a commercial TE module.

3.2.1 Comparison of the models

Before optimizing a and d, we compare the numerical results with the 1D results by taking Module A (a conventional structure; $n_1 = n_2 = 2$) as an example. The optimized TE element dimensions from the 1D analysis are $l_1^{\mathrm{p}} = 0.450$ mm and $l_2^{\mathrm{p}} = 0.744$ mm.

Figure 4 shows the voltage-current and power-current characteristics of Module A calculated using both the 1D analytical model and the 2D numerical model. The maximum power results of the analytical and numerical models are 73.5 mW and 68.1 mW, respectively. To discuss this difference, we examine the calculated temperature and electric potential distributions in both models.

Figure 5 shows the temperature, electric potential, and current density distributions for Module A when maximum power is generated. The surface temperatures T_{11} and T_{12} of the insulator are shown in Fig. 5 (a) as a function of the horizontal position x. The temperature is homogeneously distributed along the x direction, as shown in the contour plot; however, T_{11} and T_{12} are not completely constant due to the difference in the thermal conductivities of the TE elements and the Peltier effect that generates and absorbs heat according to the current at the junctions. The voltage drop caused by the current through electrodes is negligible, as shown in Fig. 5 (b), although the current density increases at the electrodes.

The temperature difference between T_{11} and T_{12} (T_{11}–T_{12}) was approximately 5 K, which is not identical to that obtained in the 1D model because, in that calculation, the thermal resistance in the insulators was ignored, and it was assumed that no temperature difference exists inside the insulators. Although the insulators are thin and have a thermal conductivity that is 10 times higher than the TE materials, the TE power is sensitive to the temperature difference and drops drastically even if the temperature difference between both sides of the TE element decreases slightly due to the thermal resistance of the insulators. Therefore, it is important to minimize the

thermal resistance by reducing the insulator thickness and using insulators with a higher thermal conductivity.

3.2.2 Optimization of the cross-sectional area and leg length

Figure 6 shows the power obtained at $n_1 = 2$ as a function of n_2; Module A corresponds to $n_2 = 2$. The maximum power is obtained at $n_2 = 6$, where $l_1^{\mathrm{p}} = 0.462$ mm and $l_2^{\mathrm{p}} = 0.220$ mm. Based on these 1D results, two possible structures (Module B and Module C), which are equivalent in the 1D analysis, were constructed numerically. The first stage was fixed at $n_1 = 2$ as the hot side of the two modules. Both models use six p-n pairs in the second stage ($n_2 = 6$), but the first and second stages of Module B have the same width, while the two stages have different widths in Module C.

Figure 7 shows the temperature, electric potential, and current density distributions in Module B, and Fig. 8 shows the corresponding results in Module C. Table 3 lists the dimensions of these modules and their performance.

Module C exhibited a higher power than that of Module B, and we focus on the surface temperatures T_{11} and T_{12} of the intermediate insulators in Modules B and C to study this difference in detail. The temperature difference was approximately 5 K in Module B, as in the case of Module A, while only a small temperature difference was

calculated in Module C; T_{11} in Module C was lower than that of both Modules A and B. Because the heat transfer area of the intermediate insulator in Module C is larger than those of Modules A and B, the heat transfer rate from the hot to cold side is increased. As a result, E_1 in Module C was higher than that in Module B, as shown in Table 3. Furthermore, in Module C, it was found that the temperature at the hot side of the second stage, T_{12}, exceeded the target temperature of 500 K. Thus, E_2 in Module C was also higher than that in Module B, although T_{12} decreases with increasing distance from the module center in the x direction. These high E_1 and E_2 values in Module C resulted in the higher power.

From this, we can conclude that the 1D heat transfer model was highly simplified, but partly reasonable, especially when each cascade module stage has a uniform width (e.g., Modules A and B). However, we should also consider the thermal resistance of the insulator to analyze the module performance in more detail.

As listed in Table 3, the power of Modules B and C is superior to that of Module A, but it is difficult to differentiate between Modules B and C as their performance will depend on the operating conditions and circumstances.

Module B has an advantage of a compact structure; if there is surplus heat, it would be better to fabricate a larger number of modules for the TE generating system without

using a large amount of material per module. Furthermore, it is possible that Module B achieves a higher power because the thermal resistance of the insulators can be reduced in this design.

Module C will be effective when the cooling capability is limited because the cooling surface area in the second stage is larger than that of Module B. In this work, calculations were performed under a constant temperature condition, which assumes that an ideal heat sink with an infinitely large heat capacity is used. Considering the practical limitations in the cooling capacity, however, the temperature at the cold side may rise above the target temperature in the case of a small cooling area, as in Modules A and B.

Module C is thus the most practical for the purposes of obtaining the highest power from the heat source with a finite heat capacity. It is necessary that we have to optimize the cascade structure to the given external circumstances including the heat source size, heat sink, and material properties. Numerical simulation is one effective method for optimizing the module structure in detail.

CONCLUSIONS

This work reported a calculation method and results for the optimization of cascade structures and compared 1D analytical and 2D numerical calculations.

The TE material dimensions and number of p-n pairs were optimized using 1D analysis, and the optimal condition depended on the particular combination and performance of the TE materials. When TE materials with a higher performance were used in the cascade module, the optimization procedure became crucial and was effective in enhancing the conversion efficiency.

Numerical calculations based on the finite volume method were used to evaluate the efficiencies of two possible modules, Modules B and C, which are equivalent in the 1D analysis. The powers of Modules B and C were calculated to be 93.6 mW and 98.4 mW, respectively, and were superior to that of Module A (P = 68.1 mW). The characteristics of the two models were examined.

We emphasized the importance of module design as well as development of TE materials. It is expected that this work will encourage to open up new application areas which recover unused heat, in particular, over a wide temperature range such as 1200-300 K.

ACKNOWLEDGEMENTS

The authors acknowledge financial support from the Japan Science and Technology Agency (JST) - Core Research of Evolutional Science and Technology (CREST) project led by Prof. K. Koumoto at Nagoya University, Japan. They also thank Prof. H. Anno and Dr. R. Funahashi for useful discussions.

REFERENCES

1. D.M. Rowe, J. Smith, G. Thomas, G. Min, J. Electron. Mater. 40, 784 (2011).

2. L.A. Rosendahl, P.V. Mortensen, A.A. Enkeshafi, J. Electron. Mater. 40, 1111 (2011).

3. M. Chen, Y. Sasaki, R.O. Suzuki, Mater. Trans. 52, 1549 (2011).

4. N. Wang, L. Han, H. He, N. Park, K. Koumoto, Energy Environ. Sci. 4, 3676 (2011).

5. D. Kraemer, B. Poudel, H.P. Feng, J.C. Caylor, B. Yu, X. Yan, Y. Ma, X. Wang, D. Wang, A. Muto, K. McEnaney, M. Chiesa, Z. Ren, G. Chen, Nature Materials 10, 532 (2011).

6. T.C. Harman, J. Appl. Phys. 29, 1471 (1958).

7. L. Zhang, T. Tosho, N. Okinaka, T. Akiyama, Mater. Trans. 49, 1675 (2008).

8. R. Funahashi, Sci. Adv. Mater. 3, 682 (2011).

9. H. Kaibe, I. Aoyama, M. Mukoujima, T. Kanda, S. Fujimoto, T. Kurosawa, H. Ishimabushi, K. Ishida, L. Rauscher, Y. Hata, S. Sano, Proc. 24th Int. Conf. Thermoelectrics 2005 (ICT2005), p.242.

10. D.M. Rowe, CRC Handbook of Thermoelectrics, (CRC Press, Boca Raton, 1995).

11. M. Chen, L.A. Rosendahl, T.J. Condra, Int. J. Heat Mass Transf. 54, 345 (2011).

12. M. Chen, S.J. Andreasen, L.A. Rosendahl, S.K. Kær, T.J. Condra, J. Electron. Mater. 39, 1593 (2010).

13. R.O. Suzuki, Y. Sasaki, T. Fujisaka, M. Chen, J. Electron. Mater. 41, 1766 (2012).

14. N. Tsujii, J.H. Roudebush, A. Zevalkink, C.A. Cox-Uvarov, G.J. Snyder, S.M. Kauzlarich, J. Solid State Chem. 184, 1293 (2011).

15. W. Luo, H. Li, F. Fu, W. Hao, X. Tang, J. Electron. Mater. 40, 1233 (2011).

16. C. Wan, Y. Wang, N. Wang, W. Norimatsu, M. Kusunoki, K. Koumoto, J. Electron. Mater. 40, 1271 (2011).

17. R. Zhang, C. Wang, J. Li, K. Koumoto, J. Am. Ceram. Soc. 93, 1677 (2010).

18. Japan Society of Mechanical Engineering, JSME Data Book Heat Transfer, 4th ed. (Maruzen, Tokyo, 1986).

Table Captions

Table 1 Choice of thermoelectric materials for three-stage cascade-type modules

Table 2 Optimized parameters and their performance

Table 3 Dimensions of modules and their performance

Figure Captions

Fig. 1 Illustration of a cascade-type thermoelectric module

Fig. 2 Workflow of the numerical calculation

Fig. 3 Contour plots of the efficiency against the number of p-n pairs of the second and third stages in a three-stage module at $n_1 = 100$; (a) Case 1, (b) Case 2, and (c) Case 3

Fig. 4 Voltage-current and power-current characteristics of Module A calculated using a one-dimensional analytical model (1D) and numerical model (2D)

Fig. 5 (a) Temperature profile, (b) electric potential profile, and (c) current density profile of Module A

Fig. 6 Power as a function of the number of p-n pairs of the second stage in a two-stage cascade module at $n_1 = 2$

Fig. 7 (a) Temperature profile, (b) electric potential profile, and (c) current density profile of Module B

Fig. 8 (a) Temperature profile, (b) electric potential profile, and (c) current density profile of Module C

Table 1 Choice of thermoelectric materials for three-stage cascade-type modules

	Temperature range	Case 1	Case 2	Case 3
$Ca_3Co_4O_9$ (p)	1200–800 K	ZT = 0.45	ZT = 0.45	ZT = 0.71
$Ba_8Al_{16}Si_{30}$ (n)	1200–800 K	ZT = 0.40	ZT = 0.40	ZT = 0.47
$MnSi_{1.73}$ (p)	800–500 K	ZT = 0.27	ZT = 0.27	ZT = 0.52
$Mn_3Si_4Al_3$ (n)	800–500 K	ZT = 0.15	–	ZT = 0.56
TiS_2 (n)	800–500 K	–	ZT = 0.29	–
Bi_2Te_3 (p)	500–300 K	ZT = 0.93	ZT = 0.93	ZT = 0.93
TiS_2 (n)	500–300 K	ZT = 0.16	ZT = 0.16	–
$SrTiO_3$ (n)	500–300 K	–	–	ZT = 1.0

Table 2 Optimized parameters and their performance

Case	n_1	n_2	n_3	l_1^{p} (mm)	l_2^{p} (mm)	l_3^{p} (mm)	I (A)	P (W)	η (%)
1-A	100	100	100	0.491	0.440	0.722	0.447	6.37	7.97
1-B	100	95	299	0.501	0.470	0.212	0.409	7.77	9.72
2-A	100	100	100	0.489	0.425	0.717	0.456	6.75	8.43
2-B	100	100	297	0.501	0.431	0.212	0.410	8.10	10.1
3-A	100	100	100	0.486	0.380	0.781	0.784	12.7	15.9
3-B	100	114	275	0.517	0.333	0.201	0.670	15.7	19.6

Table 3 Dimensions of modules and their performance

	n_1	n_2	d_1 (mm)	d_2 (mm)	I (A)	E_1 (mV)	E_2 (mV)	P (mW)	η (%)
Module A	2	2	3.07	1.27	0.491	59.0	79.7	68.1	4.40
1D analysis	2	2	–	–	0.510	61.0	83.0	73.5	4.59
Module B	2	6	2.99	1.43	0.397	84.8	151	93.6	6.04
Module C	2	6	2.99	4.29	0.407	86.7	155	98.4	6.21
1D analysis	2	6	–	–	0.412	88.0	157	101	6.31

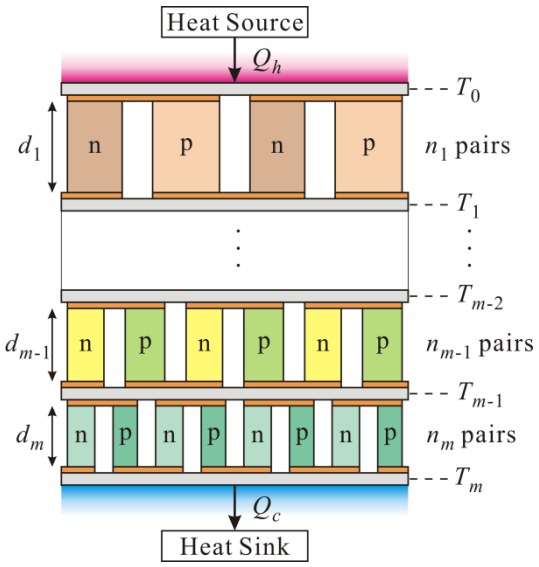

Fig. 1 Illustration of a cascade-type thermoelectric module

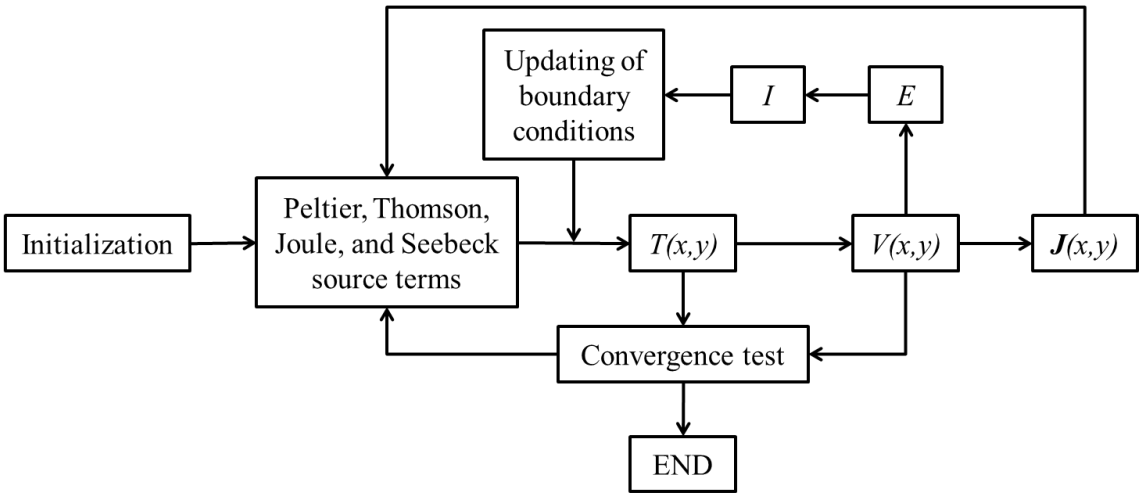

Fig. 2 Workflow of the numerical calculation

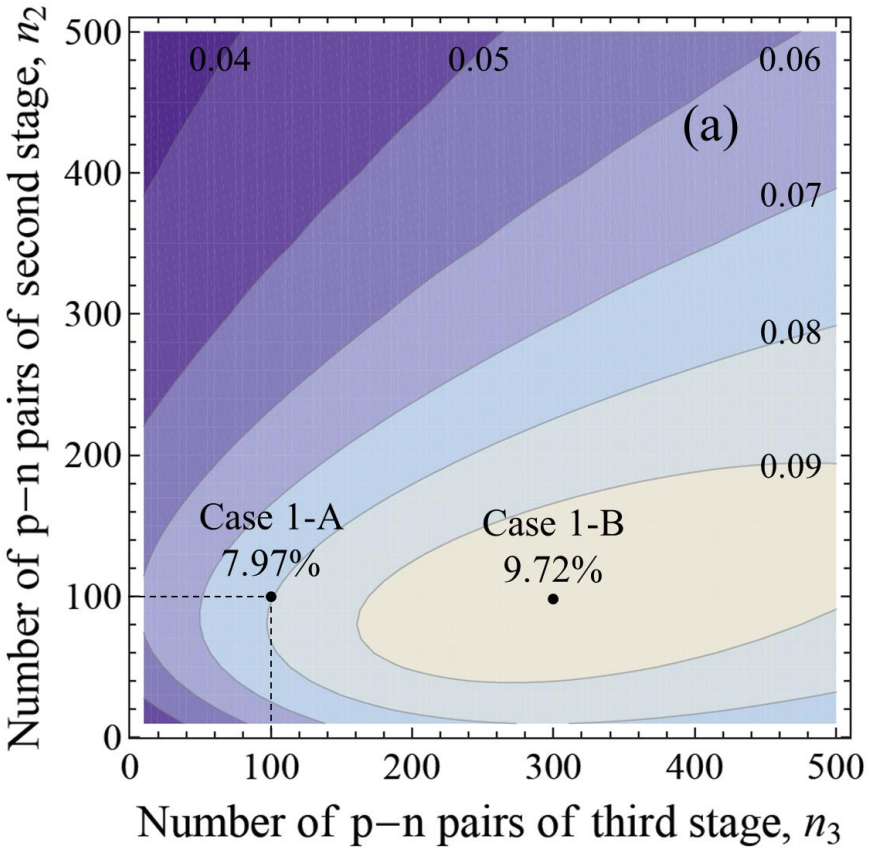
0.04
0.05
0.06
(a)
0.07
0.08
0.09
Case 1-A
7.97%
Case 1-B
9.72%
Number of p−n pairs of second stage, n_2
Number of p−n pairs of third stage, n_3
0
100
200
300
400
500

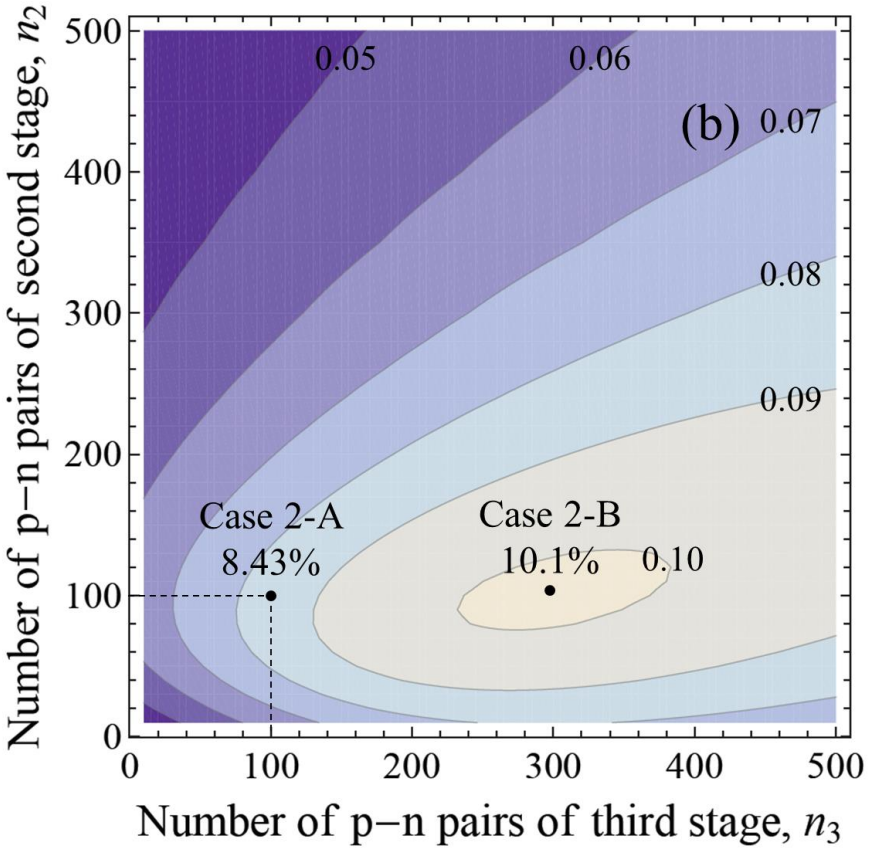
0.05
0.06
(b)
0.07
0.08
0.09
0.10
Case 2-A
8.43%
Case 2-B
10.1%
Number of p−n pairs of second stage, n_2
Number of p−n pairs of third stage, n_3
0
100
200
300
400
500

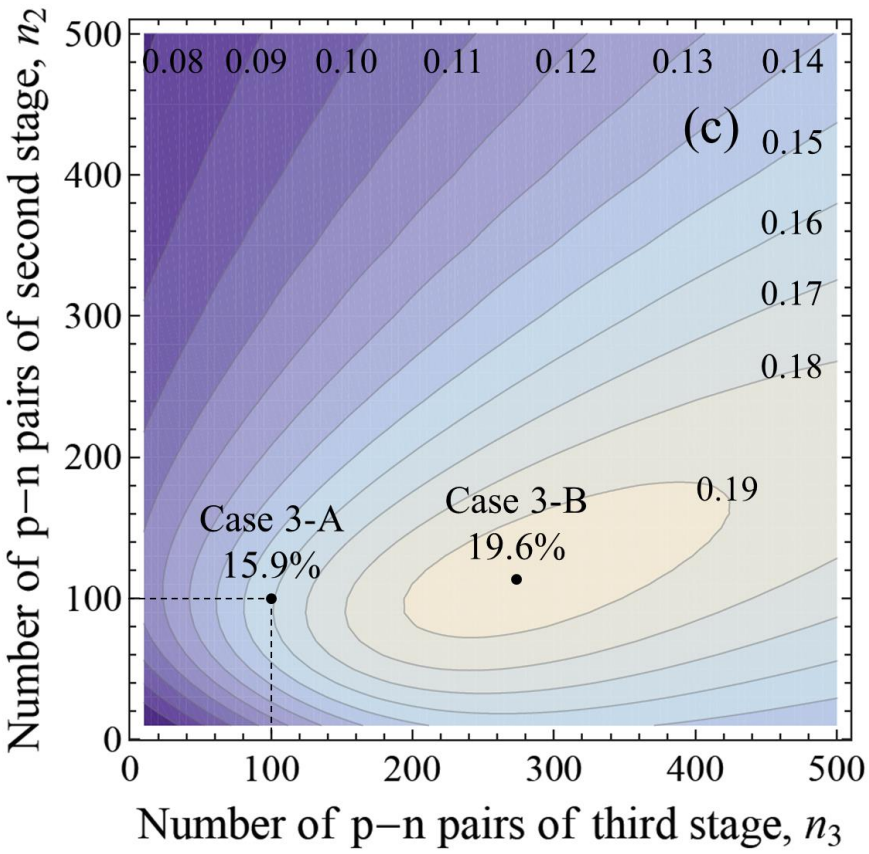

Fig. 3 Contour plots of the efficiency against the number of p-n pairs of the second and third stages in a three-stage module at n_1 = 100; (a) Case 1, (b) Case 2, and (c) Case 3

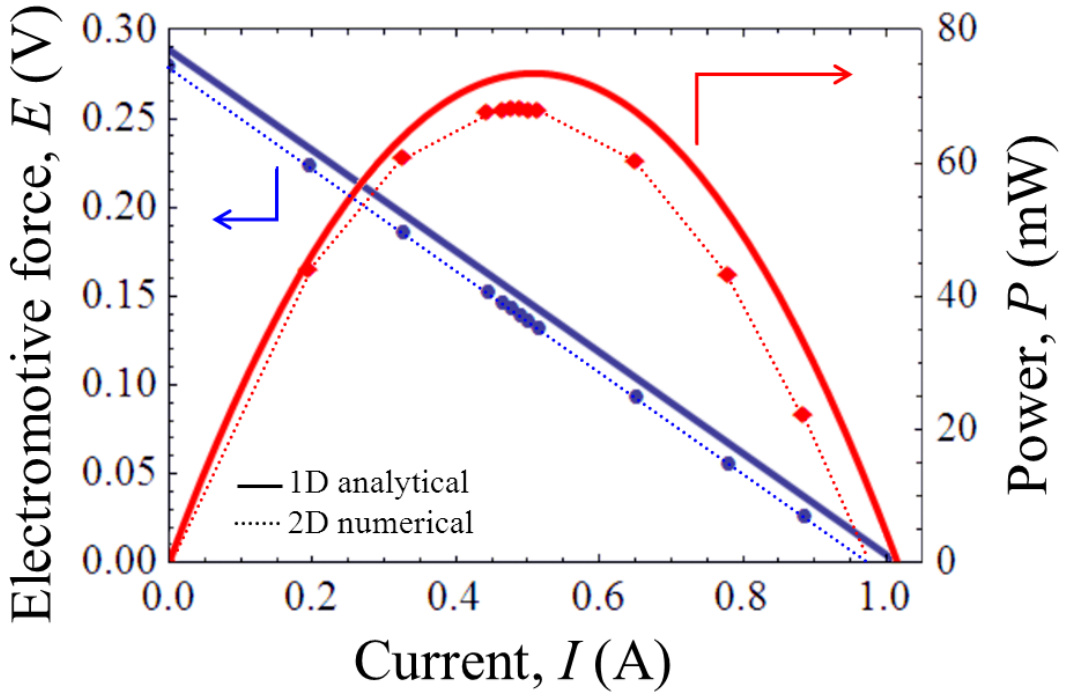

Fig. 4 Voltage-current and power-current characteristics of Module A calculated using a one-dimensional analytical model (1D) and numerical model (2D)

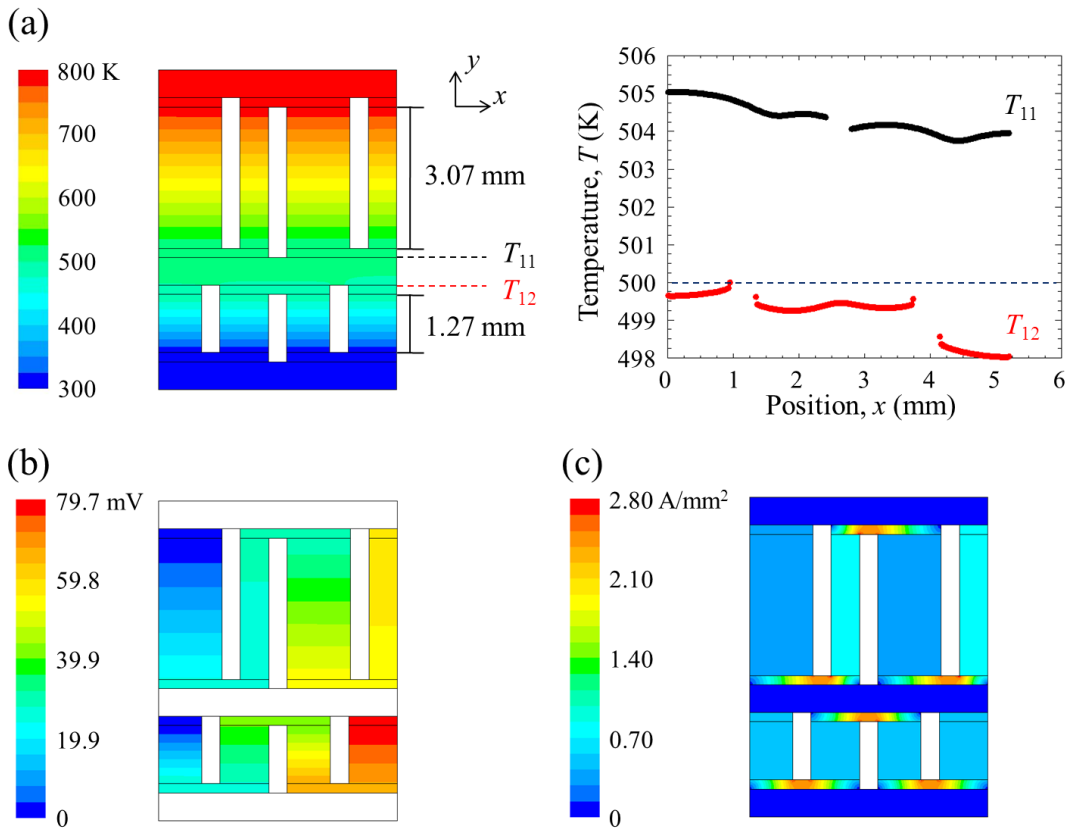

Fig. 5 (a) Temperature profile, (b) electric potential profile, and (c) current density profile of Module A

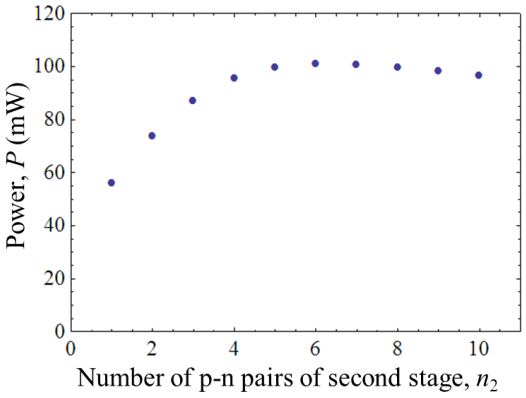

Fig. 6 Power as a function of the number of p-n pairs of the second stage in a two-stage cascade module at $n_1 = 2$

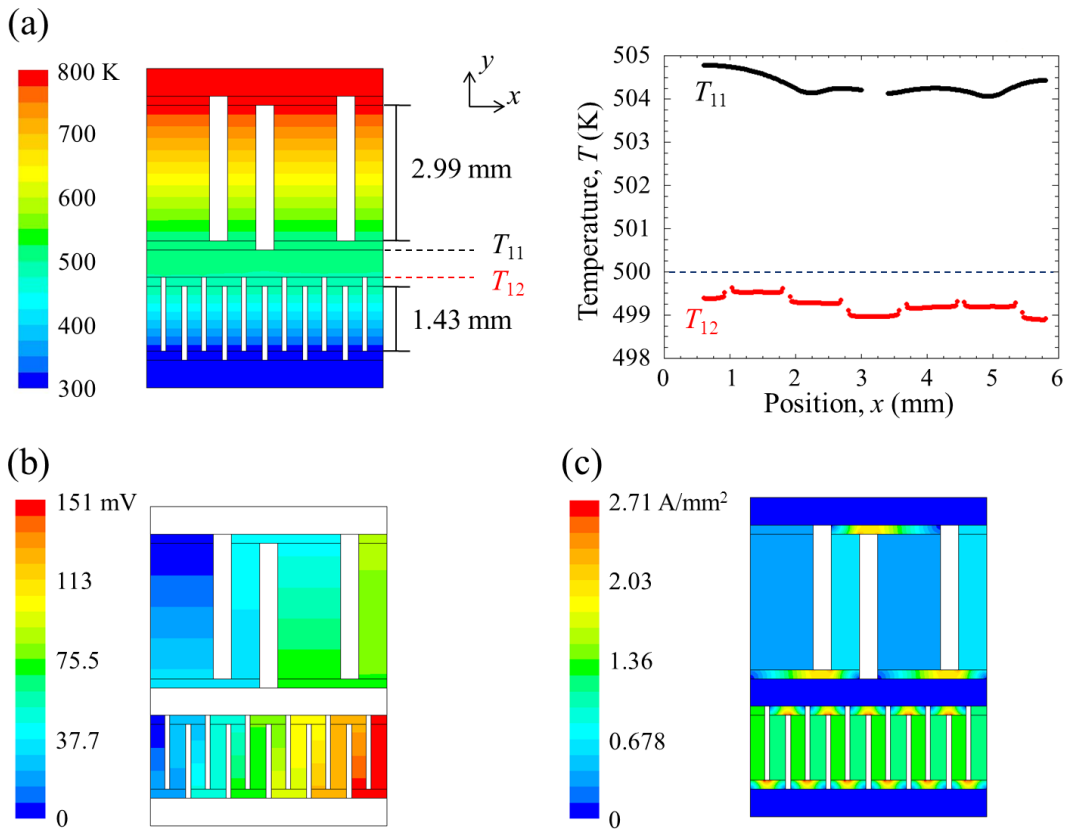

Fig. 7 (a) Temperature profile, (b) electric potential profile, and (c) current density profile of Module B

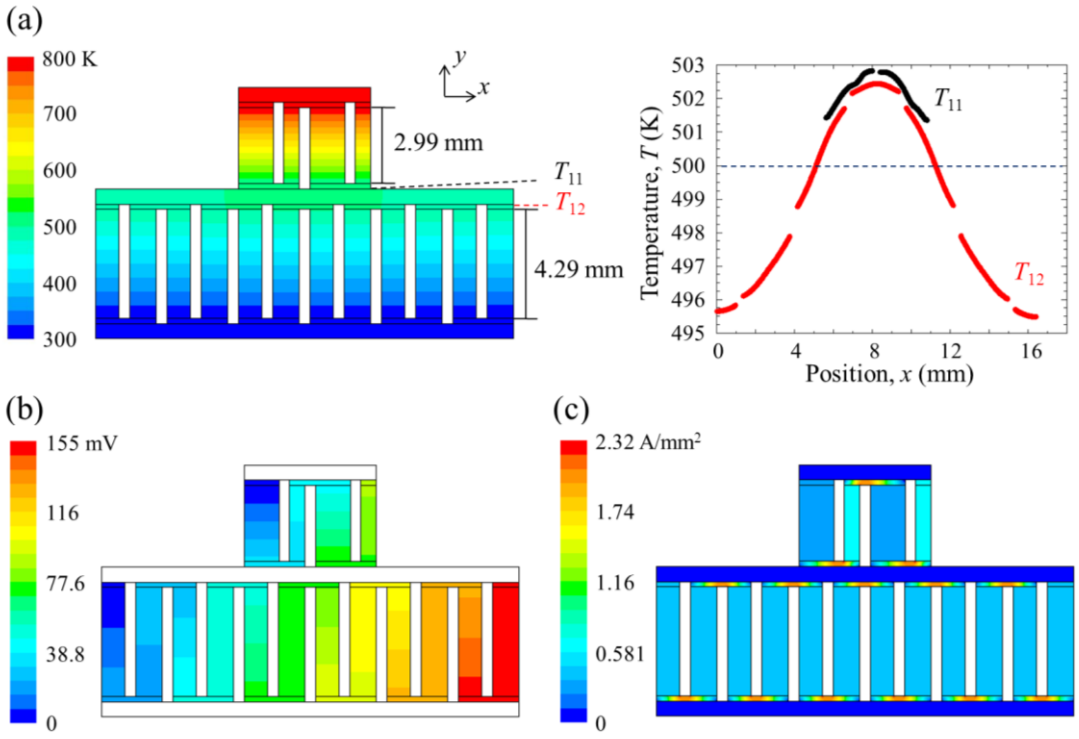

Fig. 8 (a) Temperature profile, (b) electric potential profile, and (c) current density profile of Module C